Korean J. Chem. Eng., 37(4), 688-697 (2020)
DOI: 10.1007/s11814-020-0483-8

pISSN: 0256-1115
eISSN: 1975-7220

Simultaneous NO/SO_2 removal by coconut shell char/CaO from calcium looping in a fluidized bed reactor

Boyu Li*, Yingjie Li*,†, Wan Zhang*, Yuqi Qian*, and Zeyan Wang**

*School of Energy and Power Engineering, Shandong University, Jinan 250061, China
**State Key Laboratory of Crystal Materials, Shandong University, Jinan 250100, China
(*Received 24 August 2019 • accepted 5 January 2020*)

Abstract−A simultaneous NO_x/SO_2 removal system using bio-char and CaO combined with calcium looping process for CO_2 capture was proposed. The simultaneous NO/SO_2 removal performance of coconut shell char/CaO experienced CO_2 capture cycles was investigated in a fluidized bed reactor. The effects of reaction temperature, mass ratio of CaO to coconut shell coke, CaO particle size and number of CO_2 capture cycles from calcium looping process were discussed. The NO removal efficiency of char is improved under the catalysis of CaO. The reaction temperature plays an important role in the simultaneous NO/SO_2 removal. Coconut shell char/CaO achieve the highest NO and SO_2 removal efficiencies at 825 °C, which are 98% and 100%, respectively. The mass ratio of CaO to coconut shell char of 60 : 100 is a good choice for the simultaneous NO/SO_2 removal. Smaller CaO particle size contributes to higher NO and SO_2 removal efficiencies of coconut shell char/CaO. The NO and SO_2 removal efficiencies of coconut shell char and cycled CaO from calcium looping declined slightly with the number of CO_2 capture cycles. In addition, the Ca-based materials balance in process of simultaneous NO_x/SO_2 removal combined with calcium looping is given. The novel simultaneous NO/SO_2 removal method using bio-char and cycled CaO from calcium looping process appears promising.

Keywords: CaO, Biochar, Simultaneous NO and SO_2 Removal, Fluidization, Calcium Looping

INTRODUCTION

CO_2, which has been thought as the main gas that contributes to climate change, has an increasing emissions in recent years [1]. Therefore, reducing the concentration of CO_2 in the atmosphere has become a supreme task and many studies for this have been conducted [2,3]. CO_2 capture for coal-fired plant arouses increasing attention because it is one of the main CO_2 emission sources [4]. The calcium looping process, i.e., carbonation/carbonation cycles of CaO, as one of the promising CO_2 capture technologies for coal-fired plants, has been extensively studied [5-7]. CO_2 in the flue gas from a coal-fired power plant is captured by CaO derived from limestone to form $CaCO_3$ in a carbonator at about 600-700 °C, as shown in Eq. (1). Then the generated $CaCO_3$ is sent to a calciner at above 800 °C in which $CaCO_3$ is decomposed to CaO and CO_2 under O_2/CO_2 or O_2/steam combustion, as presented in Eq. (2). The highly concentrated CO_2 from the calciner is stored and the regenerated CaO returns to the carbonator for the next CO_2 capture cycle [8,9]. Fresh limestone is added and the spent sorbent is discharged from the carbonator [10]. Calcium looping process is widely recommended owing to the high CO_2 capture efficiency, low operating cost and abundant raw materials [11,12].

$$CaO+CO_2 \rightarrow CaCO_3 \quad (1)$$

$$CaCO_3 \rightarrow CaO+CO_2 \quad (2)$$

In the calcium looping system, not only is CO_2 captured but SO_2 is removed by CaO in the carbonator [13], as shown in Eq. (3).

$$CaO+SO_2+1/2O_2 \rightarrow CaSO_4 \quad (3)$$

However, when SO_2 and CO_2 are simultaneously introduced to the carbonator, SO_2 appreciably decreases the CO_2 capture capacity of CaO during the multiple cycles, although SO_2 concentration is significantly lower than CO_2 concentration in the flue gas [14,15]. The compact $CaSO_4$ product layer formed by sulfation of CaO impedes CO_2 diffusion through the layer, which is not beneficial for the carbonation of CaO [16]. It means that the presence of SO_2 should be avoided to achieve high CO_2 capture efficiency in the calcium looping process. Thus, SO_2 should be removed before the flue gas goes into the carbonator [17].

Besides CO_2 and SO_2, NO_x is another harmful gas in the flue gas, but NO_x cannot be directly removed in the calcium looping process. Denitration in coal-fired power plants is dominated by selective catalytic reduction (SCR), since it can reach NO removal efficiency of over 90% at a relatively low temperature [18]. However, SCR is hard to be a perfect way due to the high cost, easy poisoning of catalyst, ammonia slip, and so on [19-21]. In this case, it seems attractive to develop a new NO removal method to achieve high efficiency, good safety and low cost. Char derived from coal or biomass, which is characterized by abundant resources and low price, has been previously reported to remove NO [22-24]. Guo et al. [25] studied the NO removal by chars in a fixed bed reactor, and found the best-performing lignite char only had a 50% removal efficiency at about 850 °C. The NO removal by sole char is not enough to meet the stringent emission standard for coal-fired power plants (e.g.,

†To whom correspondence should be addressed.
E-mail: liyj@sdu.edu.cn

50 mg/Nm^3 in China). CaO can improve the NO_x reduction by reducing substances such as char and CO. Zhao et al. [26] prepared lignite char impregnated by calcium nitrate solution and found the NO removal efficiency of the treated char reached 90% above 800 °C when the CaO loading was 2 wt%. Wang et al. [27] found the NO removal efficiency of cement raw meal and bituminous coal char almost doubled compared with that of bituminous coal char, and CaO in cement raw meal was maybe a catalyst for NO removal by coal char. Wang et al. [28] studied the effect of CaO on the reduction of NO by CO at 1,000 °C, and found the NO reduction efficiency was about 30% in the presence of CaO, while that was almost 0% in the absence of CaO. Wen et al. [29] calculated NO reduction reactions by quantum chemistry method and pointed out the existence of Ca decreased the energy barrier of NO reduction by char. Deshpande [30] proposed the Cal-C reactor, a modified carbonator by introducing coal char, where NO_x could be reduced by char under the catalysis of CaO at 650-700 °C.

Zhong et al. [31] investigated NO removal by different coal chars in a dropping-tube furnace at 900-1,100 °C and found larger specific surface of coal char could lead to better NO removal performance. Dong et al. [32] investigated the NO removal by three kinds of bio-char (sawdust, corn straw and rice husk) and bituminous char in a fixed bed reactor. The results clarified the reactivity with NO of the four chars following the order: sawdust>corn straw>rice husk>bituminous coal, which agreed with the order of their specific surface areas. Wang et al. [33] prepared carbide slag pellets by biomass templating to remove SO_2/NO and found the pellets showed the highest removal efficiency at 825-875 °C. Thus, biochar may be a good choice for NO_x removal due to its large specific surface area.

A simultaneous NO_x/SO_2 removal system using biochar/CaO combined with calcium looping process for CO_2 capture is proposed in this work, as shown in Fig. 1. This system includes a circulating fluidized bed (CFB) boiler, NO_x/SO_2 removal reactor, carbonator and calciner. The carbonator and the calciner involve the calcium looping process for CO_2 capture. A part of SO_2 is removed in the CFB boiler by CaO from the carbonator of the calcium looping process. Then high-temperature (850-950 °C) flue gas from boiler containing CO_2, NO_x and little SO_2 is introduced into the NO_x/SO_2 removal reactor, where most of NO_x and SO_2 are simultaneously removed by biochar and CaO from the carbonator. Lastly, the flue gas with little CO generated by biochar oxidization from the NO_x/SO_2 removal process is sent into the carbonator for CO_2 capture. At the same time, a little air is introduced into the carbonator for CO combustion. In this system, NO_x, SO_2 and CO_2 are removed by the biochar and CaO, which avoids the negative effect of SO_2 on CO_2 capture. Moreover, using CaO from calcium looping for the simultaneous NO_x/SO_2 can further recycle the spent CaO, save the fresh CaO and reduce the cost. However, the simultaneous NO_x/SO_2 removal performance of biochar and CaO from the calcium looping cycles has rarely been reported. The effect of CaO experienced CO_2 capture cycles on NO_x removal by biochar has been also not reported.

The coconut is a common fruit with a huge yield of nearly 60 million tons every year, which results in a low price and abundant production of coconut shell [34,35]. In this work, coconut shell char was chosen as a representative biochar. The simultaneous removal performance of NO and SO_2 by coconut shell char/CaO was studied in a fluidized bed reactor. The effects of the reaction temperature, mass ratio of CaO to coconut shell char, CaO particle on the simultaneous NO/SO_2 removal by coconut shell char/CaO were discussed. The influence of CaO experienced multiple CO_2 capture cycles on NO_x removal by coconut shell char was also determined.

EXPERIMENTAL

1. Materials

Limestone was used as CaO precursor. The chemical components of the calcined limestone detected by X-ray fluorescence (XRF) are shown in Table 1. The calcined limestone was denoted by CaO. CaO was crushed and screened to three particle size ranges: 0.180-

Table 1. Chemical components of calcined limestone (wt%)

CaO	MgO	Al_2O_3	K_2O	SiO_2	Fe_2O_3	SrO
95.28	1.53	0.38	0.25	2.25	0.28	0.03

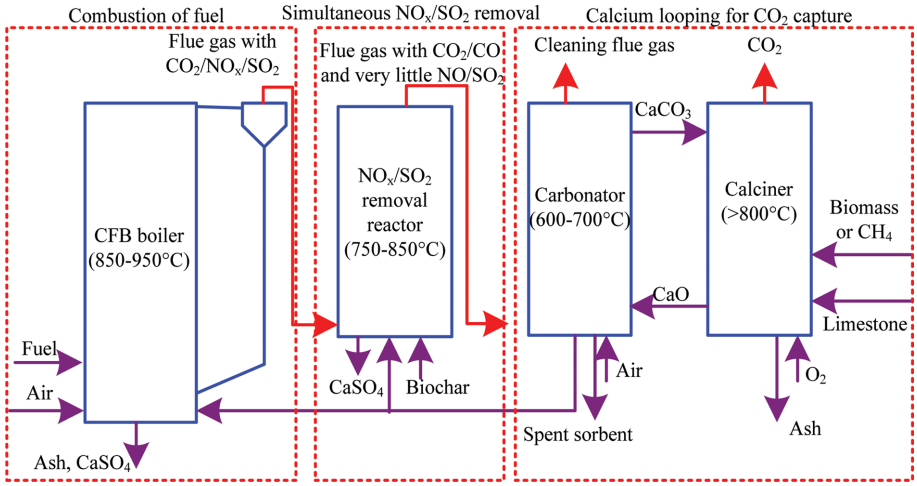

Fig. 1. Schematic process of simultaneous NO_x/SO_2 removal by biochar/CaO combined with calcium looping for CO_2 capture.

Table 2. Elementary analysis of CSC on air dry basis (wt%)

C	H	O	N	S	Ash
96.36	0.40	2.50	0.62	0.09	0.03

0.250, 0.250-0.425 and 0.425-0.600 mm.

The coconut shell was sampled from Hainan province, China. It was pyrolyzed at 950 °C under pure N_2 for 1 h and then coconut shell char (CSC) was obtained. CSC was sieved into a particle size of 0.180-0.425 mm. Table 2 shows the elementary analysis of CSC on air dry basis.

2. Simultaneous NO/SO_2 Removal Tests

The NO/SO_2 removal performance of CSC/fresh CaO and CSC/cycled CaO derived from calcium looping cycles was performed in a bubbling fluidized bed reactor (BFBR), as shown in Fig. 2. The furnace of BFBR was a quartz tube with an inner diameter of 32 mm and a height of 900 mm. A perforated distributor plate in the furnace was located at the bottom of the isothermal region with a length of 200 mm. An electric heater was able to heat and control the quartz tube at a temperature of 750-850 °C. The mixed gas of 500 ppm NO, 300 ppm SO_2, 14% CO_2 and 2.5% O_2 diluted by N_2 was controlled by mass flowmeters (Flowmethod FL-802). All the gas concentrations in the mixed gas were selected according to the flue gases of coal-fired fluidized bed boilers with the addition of limestone [36-38]. All the particles of samples were under a bubbling fluidization state when the total flow rate of the reaction gas was set as 2 L/min.

The BFBR was firstly heated to a specified temperature. The different gases from gas cylinders were mixed uniformly in a gas chamber and then were introduced into the BFBR through an air preheater. Then, 5 g samples were added into the BFBR through a hopper. The composition content of the exhaust gas was detected and recorded by a Testo 350 flue gas analyzer. The NO removal efficiency and SO_2 removal efficiency were defined as:

$$\eta_{NO}=\frac{C_{NO}(0)-C_{NO}(t)}{C_{NO}(0)}\times 100\% \quad (4)$$

$$\eta_{SO_2}=\frac{C_{SO_2}(0)-C_{SO_2}(t)}{C_{SO_2}(0)}\times 100\% \quad (5)$$

The cycled CaO from CO_2 capture cycles based on calcium looping process was prepared in the BFBR. First, CaO was sent into the reactor for 15 min under the mixed reaction atmosphere of 15% CO_2 and 85% N_2. The CO_2 concentration in the exhaust gas was recorded by the Testo 350 flue gas analyzer. After the carbonation of CaO, the reaction gas was switched to pure O_2 and the reactor was heated to 850 °C for the calcination of $CaCO_3$. When the concentration of CO_2 in exhaust gas decreased to 0%, the calcination was finished. Finally, CaO experienced 1 CO_2 capture cycle was obtained. CaO experienced many cycles was prepared according to the above-mentioned procedure. CO_2 capture efficiency was calculated as:

$$\eta_{CO_2}=\frac{C_{CO_2}(0)-C_{CO_2}(t)}{C_{CO_2}(0)}\times 100\% \quad (6)$$

3. Characterization

An X-ray diffractometer (XRD, RIGAKU D/Max-III) was used to determine the phase compositions of the samples after the reaction. The microstructure of the samples was observed by a scanning electron microscope (SEM, SUPRATM). The surface areas and the pore volumes of the samples were analyzed by a nitrogen absorption analyzer (Micromeritics ASAP 2020-M), which were calculated by the Brunauer-Emmett-Teller (BET) method and the Barrett-Joyner-Halenda (BJH) model, respectively. The pore size distributions of the samples were computed by BJH model.

RESULTS AND DISCUSSION

1. Effect of CaO on NO/SO_2 Removal by CSC

The NO and SO_2 removal performance of CSC/CaO (the mass ratio of CaO to CSC=60 : 100) and CSC (without addition of CaO) is shown in Fig. 3. After the addition of CSC or CSC/CaO, above 90% NO is removed and this situation maintains stably for 2,400 s. As shown in Fig. 3(a), the NO removal efficiencies of CSC/CaO

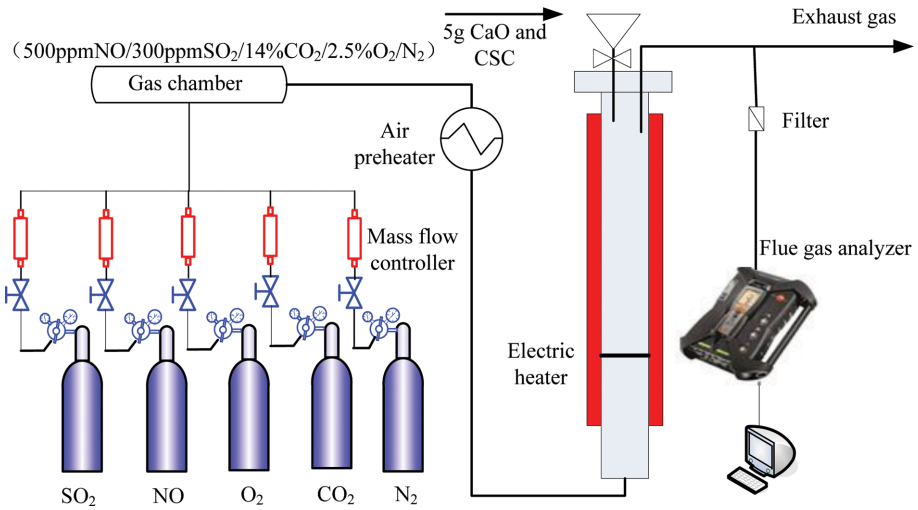

Fig. 2. Diagram of BFBR.

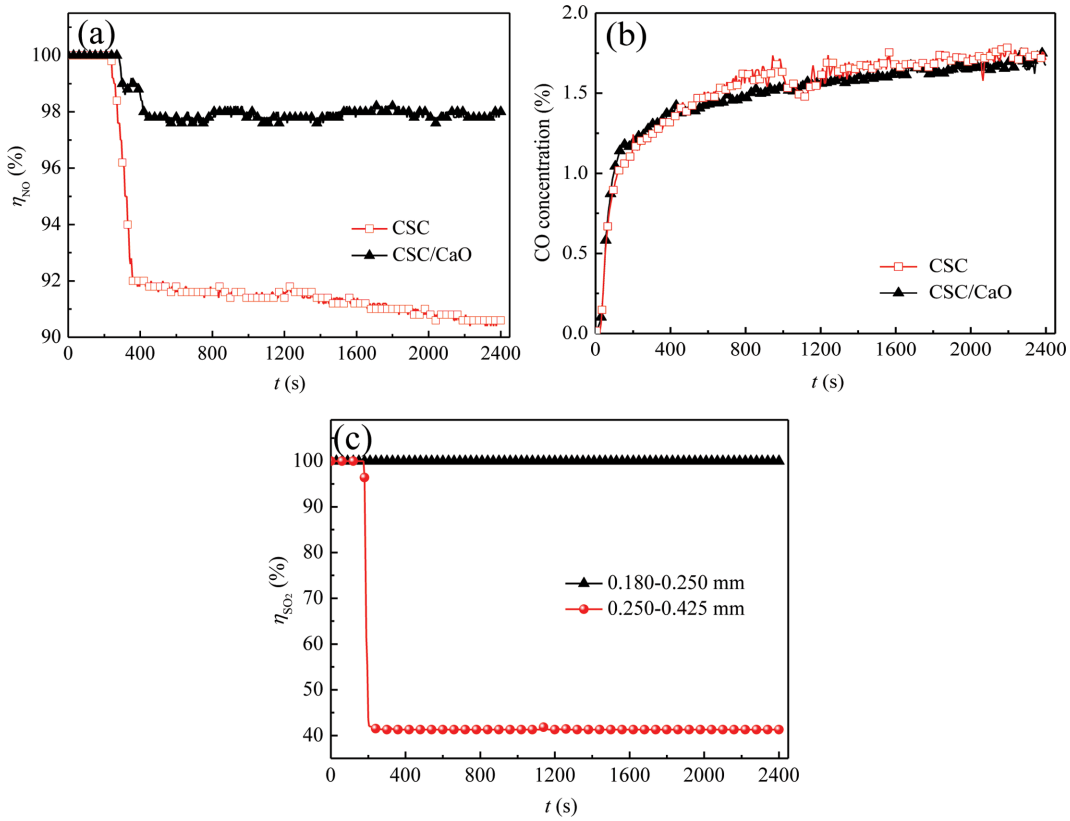

Fig. 3. Effect of CaO on NO/SO_2 removal by CSC in BFBR: (a) NO removal efficiency, (b) CO concentration in exhaust gas, (c) SO_2 removal efficiency (825 °C, 500 ppm NO/300 ppm SO_2/14% CO_2/2.5% O_2/N_2 balance, CaO particle size: 0.180-0.250 mm).

and CSC retain about 98% and 91% at 2,400 s, respectively. This indicates that the addition of CaO improves NO removal capacity of CSC in the BFBR. It is found about 1.5% CO is detected in the exhaust gas due to the main reaction between O_2 and CSC, as shown in Fig. 3(b). The addition of CaO has little effect on CO concentration in the exhaust gas. CO also reduces NO, and the reduction of NO by CO can be catalyzed by CaO [28,39,40]. The reaction process of NO reduction by char and CO under the catalysis of CaO is shown in Eqs. (7)-(10) [41,42], as follows:

$$CaO+NO \rightarrow CaO\text{-}ON \quad (7)$$

$$CaO\text{-}ON \rightarrow CaO\text{-}O^*+N^* \quad (8)$$

$$N^*+N^* \rightarrow N_2 \quad (9)$$

$$CaO\text{-}O^*+C(CO) \rightarrow CaO+CO(CO_2) \quad (10)$$

The energy barrier of the bond break of atoms N and O in the presence of CaO decreases. NO is adsorbed onto the surface and the inner pores of CaO first and then the abovementioned reac-

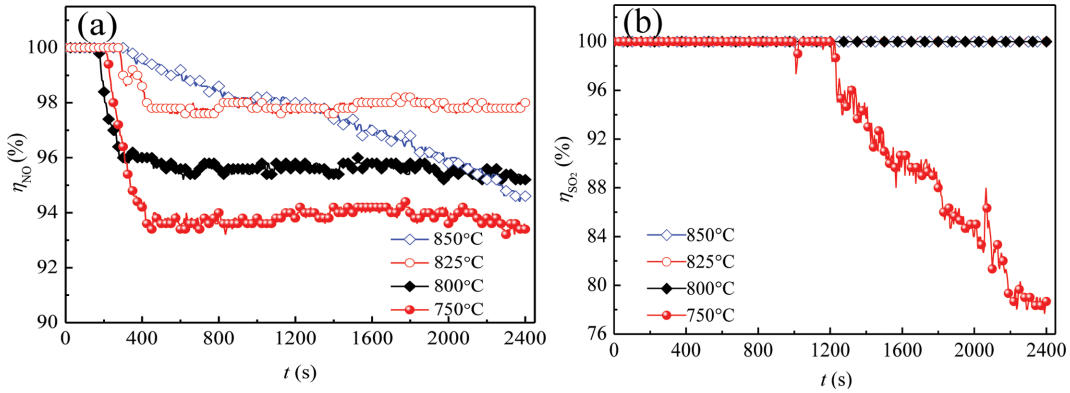

Fig. 4. Effect of reaction temperature on simultaneous NO/SO_2 removal by CSC/CaO in BFBR: (a) NO removal efficiency, (b) SO_2 removal efficiency (500 ppm NO/300 ppm SO_2/14% CO_2/2.5% O_2/N_2 balance, mass ratio of CaO to CSC=60 : 100, CaO particle size: 0.180-0.250 mm).

tions happen. Thus, the microstructure of CaO is important for the catalysis of NO reduction.

As displayed in Fig. 3(c), approximately 42% SO_2 is removed by CSC, while all SO_2 is removed by CSC and CaO. A part of SO_2 can be reduced to elemental sulfur by char, and elemental sulfur stays on the surface of char [43]. After addition of CaO, the reaction of Eq. (3) happens and SO_2 is removed completely. Thus, CaO plays the main role in SO_2 removal. Therefore, CaO improves the simultaneous NO/SO_2 removal performance of CSC.

2. Effect of Reaction Temperature on Simultaneous Removal of NO/SO_2 by CSC/CaO

The effect of the reaction temperature on simultaneous NO and SO_2 removal by CSC/CaO is illustrated in Fig. 4. The reaction temperature plays an important role in NO removal. As presented in Fig. 4(a), when the reaction temperature increases from 750 to 825 °C, the NO removal efficiency of CSC/CaO increases from about 93% to 98%. However, as the temperature rises further from 825 to 850 °C, the NO removal efficiency decreases gradually. That is maybe because the severe sintering of CaO at the high reaction temperature above 850 °C results in the blockage and collapse of pores of CaO, which decreases the catalytic action of CaO on NO reduction by CO and char. Therefore, the feasible reaction temperature for NO removal by CSC/CaO is 825 °C. As plotted in Fig. 4(b), SO_2 can be completely removed by CaO due to high molar ratio of Ca/S at the temperature of 800-850 °C. In 2,400 s, the molar ratio of Ca/S reaches 31 with the mass ratio of CaO to CSC=60 : 100. However, when the temperature is 750 °C, SO_2 removal efficiency decreases rapidly after 1,200 s. Considering the simultaneous removal of NO and SO_2, the feasible reaction temperature should be 825 °C.

Fig. 5 shows the XRD spectra of CSC/CaO after NO/SO_2 removal at 750 and 825 °C. When the reaction temperature is 750 °C, the phase compositions of CSC/CaO after NO/SO_2 removal are amorphous carbon, unreacted CaO, $CaSO_4$ and $CaCO_3$. $CaSO_4$ is generated by the sulfation of CaO. The generation of $CaCO_3$ in the reaction products indicates that the carbonation reaction of CO_2 and CaO occurs at 750 °C. The carbonation of CaO is not beneficial for SO_2 removal by CaO due to the competition. In addition, the carbonation of CaO also reduces the catalytic action of CaO on NO reduction. $CaCO_3$ is not detected in the reaction product of CSC/CaO after NO/SO_2 removal at 825 °C. The carbonation of

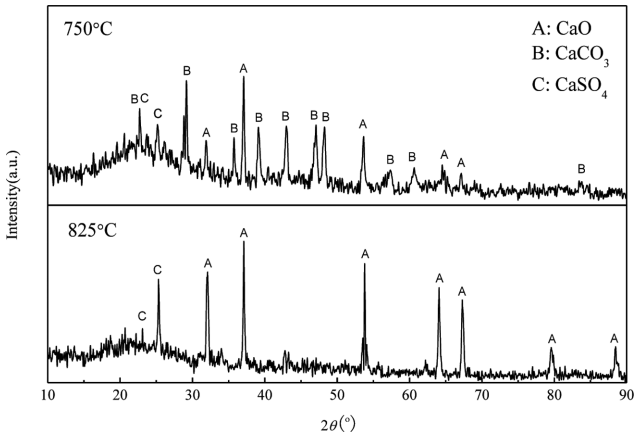

Fig. 5. XRD spectra of CSC/CaO after SO_2/NO removal reaction at 750 and 825 °C (500 ppm NO/300 ppm SO_2/14% CO_2/2.5% O_2/N_2 balance, the mass ratio of CaO to CSC=60 : 100, CaO particle size: 0.180-0.250 mm).

CaO is dictated by the thermodynamic equilibrium equation proposed by Barin [44], as presented in Eq. (11). When the concentration of CO_2 is 14%, i.e., CO_2 partial pressure of 0.14 bar, the equilibrium temperature is 1,049 K (776 °C). It means the reaction between CO_2 and CaO only happens at a temperature below 776 °C. For this reason, the carbonation of CaO does not occur at 825 °C.

$$P_{eq} = 4.137 \times 10^{7} \exp\left(-\frac{20474}{T}\right) \quad (11)$$

Therefore, it is easy to understand why the simultaneous NO/SO_2 removal efficiencies of CSC/CaO at 825 °C are higher than those at 750 °C.

3. Effect of Mass Ratio of CaO to CSC on Simultaneous Removal of NO/SO_2 by CSC/CaO

Fig. 6 presents the effect of the mass ratio of CaO to CSC on the simultaneous NO/SO_2 removal by CSC/CaO. It is found that the mass ratio of CaO to CSC has a little effect on NO removal by CSC/CaO in 1,200 s. For the different mass ratios of CaO to CSC, the NO concentrations in the exhaust gas are about 10 ppm and the corresponding NO removal efficiencies of CaO/CSC are all about 98% at 1,200 s, as shown in Fig. 6(a). When the reaction time is

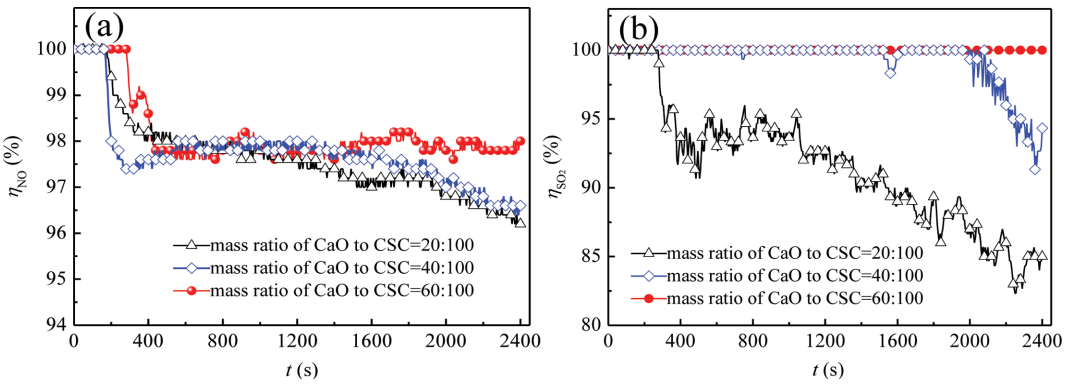

Fig. 6. Effect of mass ratio of CaO to CSC on simultaneous NO/SO_2 removal by CSC/CaO in BFBR: (a) NO removal efficiency, (b) SO_2 removal efficiency (825 °C, 500 ppm NO/300 ppm SO_2/14% CO_2/2.5% O_2/N_2 balance, CaO particle size: 0.180-0.250 mm).

above 1,200 s, the higher mass ratio of CaO to CSC leads to higher NO removal efficiency. For example, the NO removal efficiency of CSC/CaO with the mass ratio of CaO to CSC=20 : 100 at 2,400 s is about 96%, while that of CSC/CaO with the mass ratio of CaO to CSC=60 : 100 at 2,400 is still 98%. It means that the high mass ratio of CaO to CSC prolongs the reaction time corresponding to high NO removal efficiency (e.g., 98%). That is because the higher mass ratio of CaO to CSC improves the catalytic action of CaO on NO reduction by CSC. The mass ratio of CaO to CSC also has an important effect on SO_2 removal by CSC/CaO, as presented in Fig. 6(b). The higher mass ratio of CaO to CSC leads to higher molar ratio of CaO to SO_2, which is beneficial for SO_2 capture by CaO [45,46]. The high mass ratio of CaO to CSC seems beneficial for the simultaneous NO and SO_2 removal. However, when the mass ratio of CaO to CSC increases from 40 : 100 to 60 : 100, the improvement in NO and SO_2 removal efficiencies is little. Thus, it can be deduced that the improvement will be not high with increasing the mass ratio of CaO to CSC further. In a realistic application, too high mass ratio of CaO to CSC will increase the energy consumption in the NO_x/SO_2 removal reactor and the cost. Therefore, the mass ratio of CaO to CSC of 60 : 100 is recommended.

4. Effect of CaO Particle Size on Simultaneous Removal of NO/SO_2 by CSC/CaO

Fig. 7 shows the effect of CaO particle size on simultaneous NO/SO_2 removal by CSC/CaO. The NO removal capacity of CSC/CaO increases significantly with decreasing the particle size of CaO, as illustrated in Fig. 7(a). When CaO particle size is 0.180-0.250 mm, the NO removal efficiency of 98% is achieved by CSC/CaO in 2,400 s. It indicates that the smaller CaO shows higher NO removal efficiency of CSC/CaO. This is because the smaller CaO has larger surface area, which provides a higher catalytic action on NO reduction [47]. The CaO particle size has a similar effect on SO_2 removal by CaO, as presented in Fig. 7(b). When the particle size of CaO is in the range of 0.180-0.250 and 0.250-0.425 mm, the SO_2 removal efficiency is about 100% in 2,400 s. The SO_2 diffusion resistance in the smaller CaO is lower, so the smaller CaO possesses higher SO_2 removal capacity [48]. Therefore, the smaller CaO particle size not only improves the NO removal capacity but also increases the SO_2 removal capacity. However, CaO particles with smaller size are much easier to escape from the fluidized bed reactor. Thus, 0.180-0.250 mm is the recommended particle size.

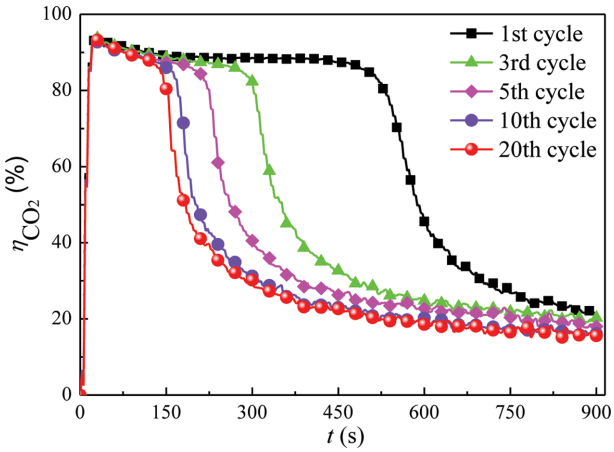

Fig. 8. CO_2 capture efficiency of CaO during 20 CO_2 capture cycles.

5. Effect of Number of CO_2 Capture Cycles on Simultaneous NO/SO_2 Removal by CSC/Cycled CaO.

Fig. 8 depicts the CO_2 capture efficiency of CaO during 20 CO_2 capture cycles based on calcium looping in BFBR. It is found that CO_2 capture capacity of CaO decreases with the number of cycles. The maximum CO_2 capture efficiency is about 90% in the first cycle. The reaction time corresponding to CO_2 capture efficiency of 90% becomes shorter with the number of cycles, which is attributed to the sintering of CaO at high temperature. The sintering results in the blockage and collapse of CaO, which is not beneficial to CO_2 capture by CaO [49-51]. Note that when the cycle number is above 5, the CO_2 capture efficiency of CaO decreases slightly with the cycle number.

The SEM images of CaO during five calcium looping cycles are illustrated in Fig. 9. The surface of initial CaO appears porous and loose. After 5 cycles, the surface of CaO seems compact and many pores disappear due to the sintering. The BET surface areas and the BJH pore volumes of CaO after different CO_2 capture cycles are shown in Table 3. The BET surface area and the BJH pore volume both drop sharply with increasing the cycle number from 0 to 5 due to the sintering. However, they appear stable as the cycle number exceeds 5. As the cycle number increases from 5 to 20,

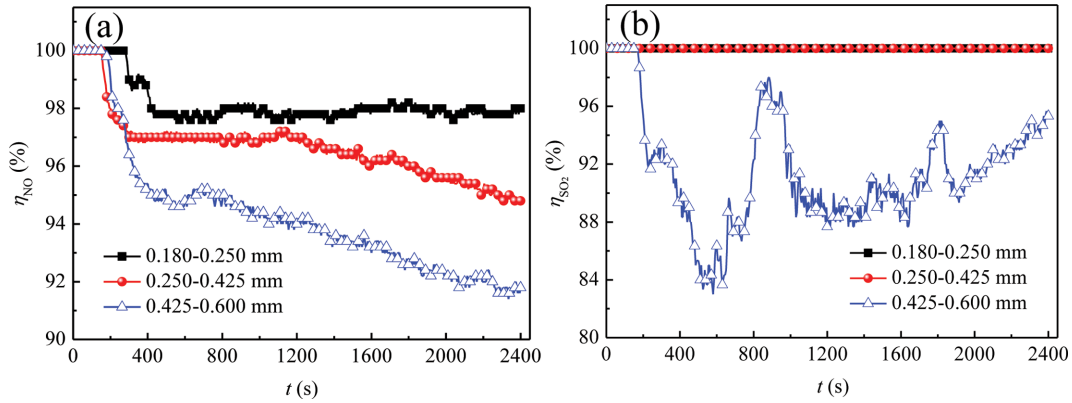

Fig. 7. Effect of CaO particle size on simultaneous removal of NO/SO_2 by CSC/CaO at 825 °C in BFBR: (a) NO removal efficiency, (b) SO_2 removal efficiency (825 °C, 500 ppm NO/300 ppm SO_2/14% CO_2/2.5% O_2/N_2 balance, the mass ratio of CaO to CSC=60 : 100).

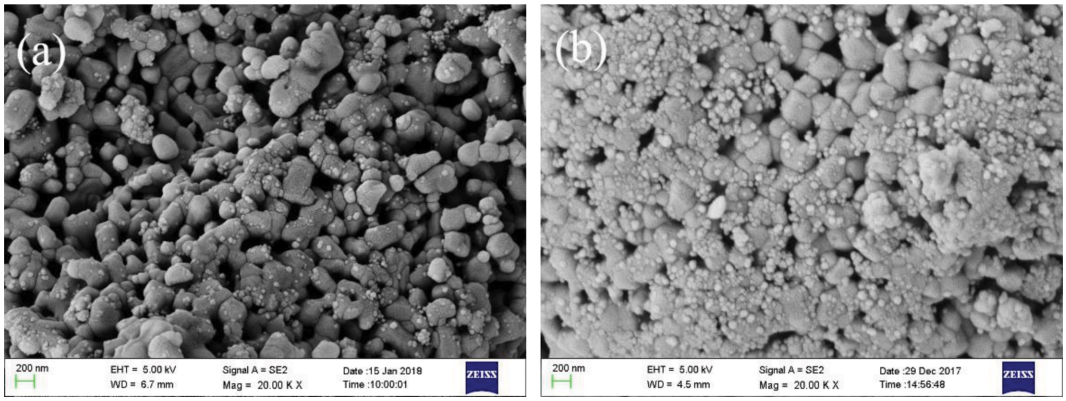

Fig. 9. SEM images of CaO after different CO_2 capture cycles: (a) initial CaO, (b) CaO after 5 cycles.

Table 3. BET surface areas and BJH pore volumes of CaO

Sample	BET surface area (m^2/g)	BJH pore volume (cm^3/g)
Initial CaO	7.15	0.055
CaO after 5 cycles	1.83	0.013
CaO after 20 cycles	1.62	0.012

the BET surface area and the BJH pore volume of CaO decreases by approximately 11% and 9%, respectively. The pore size distributions of CaO after different CO_2 capture cycles are presented in Fig. 10. As the cycle number increases from 0 to 5, the volume of pores in the measured pore size range for CaO decreases drastically. As the cycle number increases from 5 to 20, the volume of pores in 2-16 nm in diameter for CaO keeps stable, while that in 16-60 nm in diameter for CaO decreases slightly.

Fig. 11 displays the simultaneous NO/SO_2 removal by CSC/CaO after different CO_2 capture cycles. Compared with that of CSC/initial CaO, the NO removal efficiency of CSC/CaO after five cycles is slightly lower, as shown in Fig. 11(a). This is because the smaller specific surface area and pore volume of CaO after five cycles lead to a decrease in the catalytic action on NO reduction. However, it

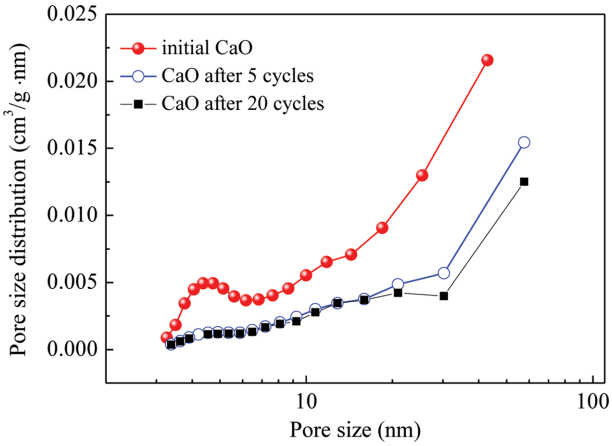

Fig. 10. Pore size distributions of CaO after different CO_2 capture cycles.

is found that NO removal efficiency of CSC/CaO after 20 cycles is slightly lower than that of CSC/CaO after 5 cycles. This may be attributed to the small difference in the microstructure of the cycled CaO (as shown in Table 3 and Fig. 10). It suggests that when the number of CO_2 capture cycles is above five, the cycled CaO has

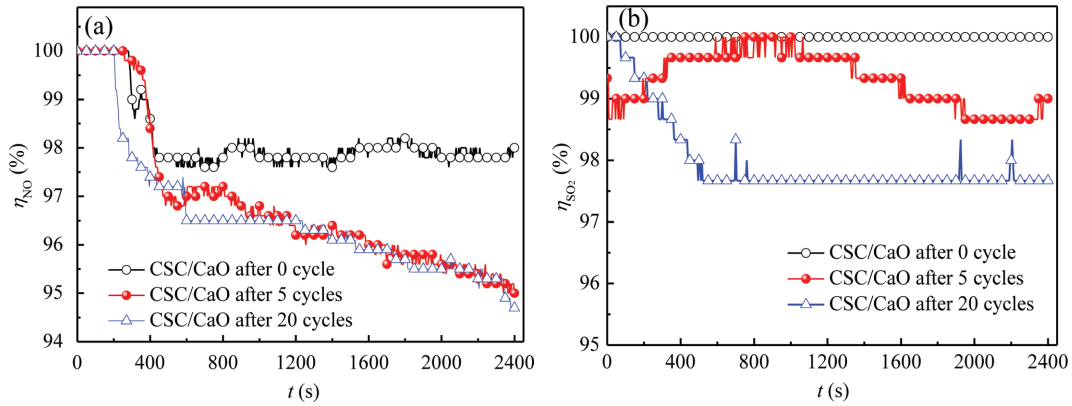

Fig. 11. Simultaneous removal performance of NO/SO_2 by CSC/CaO experienced different CO_2 capture cycles in BFBR: (a) NO removal efficiency, (b) SO_2 removal efficiency (825 °C, 14% CO_2/2.5% O_2/500 ppm NO/300 ppm SO_2/N_2 balance, the mass ratio of CaO to CSC= 60 : 100, initial CaO particle size: 0.180-0.250 mm).

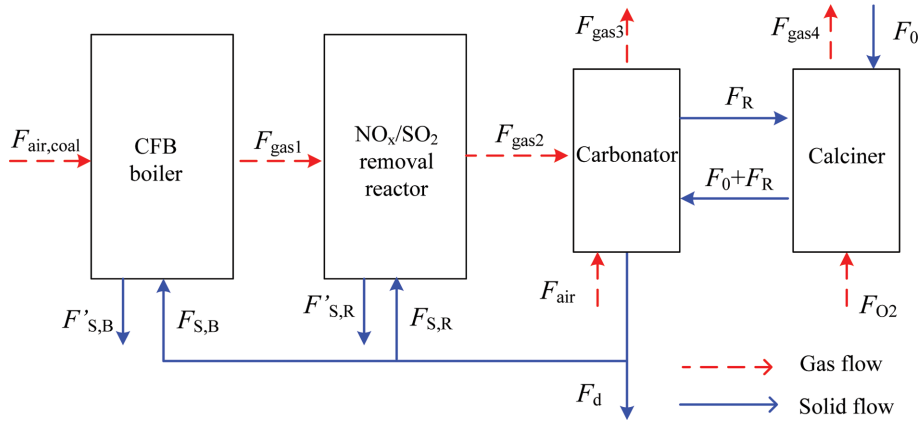

Fig. 12. Ca-based materials and gases flows (kmol/s) of the system.

little effect on NO reduction by CSC. For the same reason, the SO_2 removal efficiency of CSC/CaO after five cycles is slightly lower than that of CSC/initial CaO, as illustrated in Fig. 11(b). When the number of cycles increases from 5 to 20, the SO_2 removal efficiency of CSC/CaO drops approximately 2%. It should be noted that although the NO and SO_2 removal efficiencies of CSC/CaO after 20 cycles are lower than those of CSC/initial CaO, they are still above 94% and 97% in 2,400 s, respectively. It indicates that CSC/CaO experienced the calcium looping cycles is feasible for the simultaneous removal of NO and SO_2.

6. Ca-based Materials Balance in Process of Simultaneous NO_x/SO_2 Removal Combined with Calcium Looping

Fig. 12 presents the overall Ca-based materials flows in the process of the simultaneous NO_x/SO_2 removal by bio-char/CaO combined with calcium looping. During the calcium looping process, fresh $CaCO_3$ (F_0) is introduced into the calciner to maintain a high CO_2 capture efficiency. CaO (F_0+F_R) is sent to the carbonator for CO_2 capture, and the recycled sorbents (F_R) containing CaO and $CaCO_3$ is sent back to the calciner. The values of F_0/F_R and (F_{CO}+F_{CO2})/F_R are generally set as 0.04-0.1 and 0.5-1 to achieve a high CO_2 capture efficiency (above 85%) [52]. CO_2 capture efficiency in the carbonator is determined by the flow rates of CaO (including the fresh and the recycled CaO) flows and the average carbonation conversion (i.e., mole conversion of CaO to $CaCO_3$), X_{ave}, which is computed as Eq. (12):

$$E_{CO_2}=\frac{F_0/F_R+1}{(F_{CO}+F_{CO_2})/F_R}X_{ave} \quad (12)$$

The spent Ca-based sorbent (F_0) is discharged from the carbonator which is divided to three Ca-based material streams. A part of the discharged Ca-based stream ($F_{S,B}$) is introduced into the CFB boiler for SO_2 removal in coal combustion. In addition, a part of the discharged Ca-based stream ($F_{S,R}$) is sent to the NO_x/SO_2 removal reactor to remove NO_x/SO_2 in the presence of biochar in the flue gas. The residual part of the discharged Ca-based stream (F_d) can be recycled for the cement production. $F_{S,B}$, $F_{S,R}$ and F_d are calculated by Eqs. (13), (14) and (15), respectively, as follows:

$$F_{S,B}=\alpha F_{SO_2}E_{SO_2} \quad (13)$$

$$F_{S,R}=\beta F_{SO_2}(1-E_{SO_2}) \quad (14)$$

$$F_d=F_0-F_{S,B}-F_{S,R} \quad (15)$$

where α is usually set as the value between 2 and 3 [53]. According to the experimental results, 60 : 100 is the optimum mass ratio of CaO to biochar due to the low CaO consumption and the high removal efficiency for this novel process, so β is approximately 31. $F'_{S,B}$ and $F'_{S,R}$ are numerically equal to $F_{S,B}$ and $F_{S,R}$, respectively. According to the Ca-based materials flows, F_{gas1}, F_{gas2}, F_{gas3} and F_{gas4} are easy to obtain by Eqs. (16)-(19):

$$F_{gas1}=F_{air,coal}+F_{SO_2}(1-E_{SO_2})+F_{NO}+F_{CO_2} \quad (16)$$

$$F_{gas2}=F_{air,coal}+F_{CO}+F_{CO_2} \quad (17)$$

$$F_{gas3}=F_{air,coal}+(F_{CO_2}+F_{CO})(1-E_{CO_2})+F_{air} \quad (18)$$

$$F_{gas4}=F_{CO_2,fuel}+(F_{CO_2}+F_{CO})(1-E_{CO_2})+F_0 \quad (19)$$

CONCLUSION

A simultaneous NO_x/SO_2 removal system using bio-char and CaO combined with calcium looping process for CO_2 capture was proposed. The simultaneous NO and SO_2 removal performance of CSC/CaO was studied in a BFBR. The NO removal efficiency of char is improved under the catalysis of CaO. 825 °C is a feasible reaction temperature for the simultaneous NO/SO_2 removal by CSC/CaO. The simultaneous NO/SO_2 removal efficiencies increase as the mass ratio of CaO to CSC increases. Considering the cost of CaO and removal efficiencies, the mass ratio of CaO to CSC of 60 : 100 is recommended. CaO with smaller particle size shows a higher catalytic action on NO reduction and higher SO_2 removal capacity. When the CaO particle size is 0.180-0.250 mm, the NO and SO_2 removal efficiencies of CSC/CaO achieve 98% and 100%, respectively. The NO/SO_2 removal capacity of CSC/cycled CaO from calcium looping declines slightly with the number of CO_2 capture cycles. The decay in surface area and pore volume of CaO decreases the catalytic action of CaO on NO reduction by CO. When the number of CO_2 capture cycles is above five, the cycled CaO has little effect on NO reduction by CSC. The average NO and SO_2 removal efficiencies of CSC and CaO after 20 CO_2 capture cycles reach about 96% and 97%, respectively. The simultaneous NO/SO_2 removal by bio-char and cycled CaO from CO_2 capture cycles based

on calcium looping appears promising.

ACKNOWLEDGEMENT

This research was supported by the National Natural Science Foundation of China (51876105), the Fundamental Research Funds of Shandong University (2018JC039) and Joint Foundation of National Natural Science Foundation of China and Shanxi Province for coal-based low carbon (U1510130).

NOMENCLATURE

η_{NO} : NO removal efficiency [%]
η_{SO_2} : SO_2 removal efficiency [%]
η_{CO_2} : CO_2 capture efficiency of CaO [%]
$C_{NO}(0)$: initial NO concentration [ppm]
$C_{NO}(t)$: NO concentration in the exhaust gas from BFBR at t [ppm]
$C_{SO_2}(0)$: initial SO_2 concentration [ppm]
$C_{SO_2}(t)$: SO_2 concentrationin the exhaust gas from BFBR at t [ppm]
$C_{CO_2}(0)$: initial CO_2 concentration [%]
$C_{CO_2}(t)$: CO_2 concentration in the exhaust gas from BFBR at t [%]
P_{eq} : CO_2 equilibrium partial pressure [bar]
T : CO_2 equilibrium temperature [K]
F_0 : flow rate of fresh $CaCO_3$ [kmol/s]
F_R : flow rate of recycled sorbent excluding fresh makeup [kmol/s]
X_{ave} : average carbonation conversion of CaO
F_0/F_R : ratio of fresh sorbent flow rate to recycled sorbent flow rate
$(F_{CO}+F_{CO_2})/F_R$: ratio of total CO_2 flow rate introduced into the carbonator to recycled sorbent flow rate
$F_{S,B}$: flow rate of sorbent introduced into the boiler [kmol/s]
$F_{S,R}$: flow rate of sorbent introduced into the NO_x/SO_2 removal reactor [kmol/s]
$F'_{S,B}$: total flow rate of CaO and $CaSO_4$ discharged from the boiler [kmol/s]
$F'_{S,R}$: total flow rate of CaO and $CaSO_4$ discharged from the NO_x/SO_2 removal reactor [kmol/s]
F_{CO_2} : flow rate of CO_2 produced by coal combustion entering the carbonator [kmol/s]
F_{SO_2} : flow rate of SO_2 produced by coal combustion [kmol/s]
α : molar ratio of Ca/S in the boiler
β : molar ratio of Ca/S in the NO_x/SO_2 removal reactor
E_{CO_2} : CO_2 capture efficiency in the carbonator [%]
E_{SO_2} : SO_2 removal efficiency in the boiler [%]
F_{NO} : flow rate of NO produced by coal combustion [kmol/s]
F_{CO} : flow rate of CO produced by char [kmol/s]
F_d : flow rate of sorbent discharged from the carbonator directly [kmol/s]
F_{O_2} : flow rate of O_2 introduced into the calciner for fuel combustion [kmol/s]
$F_{air,coal}$: flow rate of air for coal combustion in the boiler [kmol/s]
F_{air} : flow rate of air for CO combustion in the carbonator [kmol/s]
F_{gas1} : flow rate of gas from boiler to NO_x/SO_2 removal reactor [kmol/s]
F_{gas2} : flow rate of gas from NO_x/SO_2 removal reactor to carbonator [kmol/s]
F_{gas3} : flow rate of gas emitted from the carbonator [kmol/s]
F_{gas4} : flow rate of gas emitted from the calciner [kmol/s]

REFERENCES

1. C. Manianglung, R. M. Pacia and Y. S. Ko, *Korean J. Chem. Eng.*, **36**, 1267 (2019).
2. D. Kang and J. W. Lee, *Appl. Catal. B*, **186**, 41 (2016).
3. H. S. Lim, D. Kang and J. W. Lee, *Appl. Catal. B*, **202**, 175 (2017).
4. A. A. Khan, G. Halder and A. K. Saha, *Korean J. Chem. Eng.*, **36**, 1090 (2019).
5. X. Ma, Y. Li, C. Chi, W. Zhang and Z. Wang, *Korean J. Chem. Eng.*, **34**, 580 (2017).
6. K.-Y. Yoo, J.-S. Park and M.-J. Park, *Korean J. Chem. Eng.*, **33**, 1153 (2016).
7. L. S. Fan, L. Zeng, W. Wang and S. Luo, *Energy Environ. Sci.*, **5**, 7254 (2012).
8. T. Shimizu, T. Hirama, H. Hosoda, K, Kitano, M. Inagaki and K. Tejima, *Chem. Eng. Res. Des.*, **77**, 62 (1999).
9. J. M. Valverde, *Chem. Eng. J.*, **228**, 1195 (2013).
10. Y. Li, X. Ma, W. Wang, C. Chi, J. Shi and L. Duan, *Chem. Eng. J.*, **316**, 438 (2017).
11. C. C. Cormos, *Energy*, **78**, 665 (2014).
12. H. Chen, N. Khalili and J. Li, *Chem. Eng. J.*, **345**, 321 (2018).
13. X. Li, W. Li, L. Wang and X. Chang, *Coal Chem. Indus.*, **46**, 17 (2018).
14. Y. Li, S. Buchi, J. And, J. R. Grace and C. J. Lim, *Energy Fuels*, **19**, 1927 (2005).
15. P. Sun, J. R. Grace, C. J. Lim and E. J. Anthony, *Energy Fuels*, **21**, 163 (2007).
16. H. Ryu, J. R. Grace and C. J. Lim, *Energy Fuels*, **20**, 1621 (2006).
17. L. Cong, Y. Zheng, J. Guo and B. Feng, *Fuel*, **127**, 124 (2014).
18. Q. Gu and X. Hu, *Clean Coal Technol.*, **21**, 77 (2015).
19. F. He, X. Deng and M. Chen, *Fuel*, **199**, 523 (2017).
20. W. Zhang, C. Lu, D. Chen, W. Deng, Q. Song, Y. Feng, W. Gong and J. Song, *Clean Coal Technol.*, **25**, 45 (2019).
21. Y. Xue, Y. Zhang, Y. Zhang, S. Zheng, Y. Zhang and W. Jin, *Chem. Eng. J.*, **325**, 544 (2017).
22. B. Wang, S.-Y. Liu, F.-Y. Li and Z.-P. Fan, *Korean J. Chem. Eng.*, **34**, 717 (2017).
23. S. Sun, J. Zhang, X. Hu, P. Qiu, J. Qian and Y. Qin, *Korean J. Chem. Eng.*, **26**, 554 (2009).
24. Z. Zhao, J. Qiu, W. Li, H. Chen and B. Li, *Fuel*, **82**, 949 (2003).
25. F. Guo and W. C. Hecker, *Symp. Combust.*, **27**, 3085 (1998).
26. Z. Zhao, W. Li and B. Li, *Fuel*, **81**, 1559 (2002).
27. S. Wang, J. Lu, Z. Hu and L. Huang, *Huazhong Univ. Sci. Tech.*, **34**, 21 (2006).
28. C. Wang, Y. Du and D. Che, *Energy Fuels*, **26**, 7367 (2012).
29. Z. Wen, Z. Wang, J. Zhou, Z. Zhou, J. Liu and K. Cen, *Combust. Sci. Technol.*, **15**, 505 (2009).
30. N. Deshpande, *Calcium and iron oxide reactivity studies for chemical looping applications of clean energy conversion*, Ph.D. Thesis, Columbus: Ohio State University (2015).
31. B. Zhong, W. Shi and W. Fu, *Fuel Process. Technol.*, **79**, 93 (2002).
32. L. Dong, S. Gao, W. Song and G. Xu, *Fuel Process. Technol.*, **88**, 707

(2007).
33. X. Wang, Y. Li, J. Shi, J. Zhao, Z. Wang, H. Liu and X. Zhou, *Fuel Process. Technol.*, **180**, 75 (2018).
34. Y. Wang, H. Qin, F. Deng, S. Gong, R. Liu, X. Zheng and H. Fang, *World Trop Agric. Inf.*, **491**, 5 (2018).
35. Z. Zhong, G. Yu, W. Mo, C. Zhang, H. Huang, S. Li, M. Gao, X. Lu, B. Zhang and H. Zhu, *RSC Adv.*, **9**, 10425 (2019).
36. A. Wilk, L. Więcław-Solny, A. Tatarczuk, A. Krótki, T. Spietz and T. Chwoła, *Korean J. Chem. Eng.*, **34**, 2275 (2017).
37. M. Cui, J. Zhou, X. Zhang, T. Li and F. Niu, *Clean Coal Technol.*, **25**, 131 (2019).
38. H. K. Nhan, M. Kwon, S. Kim and J. H. Park, *J. Mech. Sci. Technol.*, **33**, 2967 (2019).
39. K. Dam-johansen, P. Hansen and S. Rasmussen, *Appl. Catal. B*, **5**, 283 (1995).
40. M. J. Illán-Gómez, A. Linares-Solano, L. R. Radovic and C. Salinas-Martínez, *Energy Fuels*, **36**, 112 (1995).
41. B. Ulusoy, H. Wu, W. Lin, O. Karlström, S. Li, W. Song, P. Glarborg and K. Dam-Johansen, *Fuel*, **236**, 297 (2019).
42. Y. Chen, Z. Guo and Z. Wang, *J. Iron Steel Res.*, **21**, 6 (2009).
43. C. T. Ratcliffe and G. Pap, *Fuel*, **59**, 237 (1980).
44. C. Ortiz, R. Chacartegui, J. M. Valverde, A. Alovisio and J. A. Becerra, *Energy Convers. Manage.*, **149**, 815 (2017).
45. S. Q. Wang, M. Z. Liu, L. L. Sun and W. L. Cheng, *Korean J. Chem. Eng.*, **34**, 1882 (2017).
46. Y. Yang and Y. Zhang, *Appl. Energ. Technol.*, **3230**, 32 (2013).
47. R. H. Borgwardt and K. R. Bruce, *AIChE J.*, **32**, 239 (1986).
48. F. Guo and W. C. Hecker, *Symp. Combust.*, **26**, 2251 (1996).
49. X. Ma, Y. Li, L. Duan, E. Anthony and H. Liu, *Appl. Energy*, **225**, 402 (2018).
50. H. Guo, X. Kou, Y. Zhao, S. Wang, Q. Sun and X. Ma, *Chem. Eng. J.*, **334**, 237 (2018).
51. R. Sun, Y. Li, H. Liu, S. Wu and C. Lu, *Appl. Energy*, **89**, 368 (2012).
52. Y. Li, C. Zhao, H. Chen, Q. Ren and L. Duan, *Energy*, **36**, 1590 (2011).
53. L. Duan, W. Zhou, H. Li, X. Chen and C. Zhao, *Korean J. Chem. Eng.*, **28**, 1952 (2011).